The accuracy of topographical and shape analysis using three-dimensional surface scanning compared to Micro-Computed Tomography

AF Ridel [a,*], N.P. Bothma [a], L. Liebenberg [a], AC Oettlé [b,a], EN L'Abbe [a]

[a]Department of Anatomy, Faculty of Health Sciences, University of Pretoria, Pretoria, South Africa

[b]Department of Anatomy, School of Medicine, Sefako Makgatho Health Sciences University, Ga-Rankuwa, Pretoria, South Africa

* Corresponding author at: Tswelopele Building, University of Pretoria, Private Bag X323, Arcadia 0007, South Africa. Email: alison.ridel@tuks.co.za

Highlights

- Developing new methods and techniques for real-life forensic applications.
- Forty-four crania were collected and scanned using two 3D imaging modalities.
- Three-dimensional reconstructions and landmarks were compared.
- Minimal geometric discrepancies and similar shape landmarks datasets were observed.
- Similar population affinity-related mid-facial shape variations using both modalities.

Abstract

The high number of unidentified bodies recorded in South Africa annually, combined with substantial heterogeneity within the population, necessitates that innovative forensic analysis methods be developed that incorporate variations from South African groups. Although sizeable three-dimensional (3D) scanning modalities exist in osteology and anthropology, developing new advanced methods and techniques involving 3D scanning for real-life forensic applications require that the accessibility, practicality, and, more importantly, accuracy of the methods be taken into consideration. To this end, this study aimed to assess the reliability of 3D surface scanning-based topographical and shape analysis comparison to gold standard micro-focus X-ray computed tomography (micro-XCT) reconstructions for estimating population affinity.

Forty-four adult crania were collected from the Pretoria Bone Collection (PBC), University of Pretoria, South Africa. Two sets of 3D reconstructions were acquired from each cranium, namely micro-XCT scans and 3D surface scans. Three-dimensional reconstructions and landmark datasets were acquired from both scanning modalities and compared using reproducibility testing, geometric discrepancies, and shape analysis.

The minimal geometric discrepancies observed between the reconstructions suggest that both modalities will provide similar shape landmarks datasets and can be used without compromising the accuracy of the analyses at term. The statistical findings showed similar population affinity-related mid-facial shape variations analyzed across both modalities using geometric morphometric methods (GMM).

Incorporating multiple 3D scanning modalities and advanced GMM into the existing biological profile estimation will allow South African forensic anthropologists to analyze shape-related skeletal variation in a more accurate and repeatable way and provide an efficient biological profile in forensic cases.

Graphical abstract

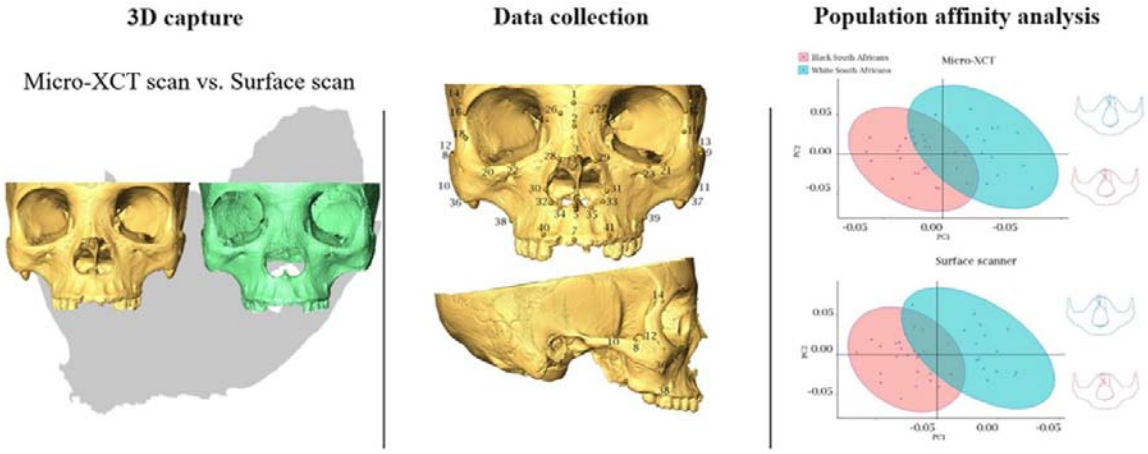

Keywords: 3D Scanning modalities; Micro-focus X-ray computed tomography (micro-XCT); Three-dimensional (3D) surface scanner; Population affinity estimation; Geometric morphometric methods (GMM)

Introduction

Today in South Africa, due to the high number of unidentified bodies each year and the population's substantial heterogeneity, a need exists to develop innovative methods that are reliable, effective, and accessible. For example, in 2023, approximately 900 bodies were reported unidentified in Gauteng mortuaries [1]. Forensic anthropologists from the Forensic Anthropology Research Centre (FARC) at the University of Pretoria collaborate with the South African Police Service (SAPS) to provide the unknown individual's biological profile. The biological profile consists of estimating sex, age, stature, and population affinity. Accurate population affinity estimation is the most critical of these components as it, in turn, directs the use of population-specific standards for sex, age, and stature [2]. Consequently, it becomes the foremost step in developing reliable biological profiles in the South African context.

Forensic anthropologists employ morphological (e.g., scoring analysis) and metric methods (e.g., Linear Discriminant Function Analysis (LDFA)) on cranial and postcranial remains to estimate the biological profile of an unknown individual. The morphological approach has been extensively criticized due to the subjectivity involved in the procedure and the fact that the reliability is highly dependent on the observer's experience [3]. Although LDFA is the most widely used metric approach and appears to be more structured and accessible than other morphological techniques, significant inter-and intra-observer discrepancies have been documented [3]. Furthermore, as LDFA requires a suite of measurements to be taken, it becomes difficult to accurately use this technique when all the necessary measures are not assessable. In contrast to classical metric approaches, Geometric morphometric Methods (GMM) are based on biological shape analysis using anatomical landmarks [4]. The utilization of GMM for population affinity estimation may be preferable to metric methods because they retain the object's geometry and analyze subtle differences among structures [4]. Furthermore, GMM could significantly overcome the exclusion of fragmented cranial or postcranial elements by creating discriminate shape matrices to analyze specific patterns not readily revealed by the traditional methods.

On account of substantial heterogeneity in the South African population and the expansion of new 3D imaging technologies available to researchers, forensic anthropologists have been developing new techniques in order to understand the morpho-phenotyping of human anatomy to improve the accuracy of biological profiles. Numerous studies already suggested that by using 3D imaging modalities, shape-related cranial variation and more particularly mid-facial shape-related variation could be used for population affinity estimation in forensic anthropological analysis [2;[5], [6], [7], [8], [9]]. Recently, Ridel and collaborators [7], [8], [9] explored population affinity-related mid-facial shape matrices variation between two South African ancestral groups using GMM applied on 3D surface meshes acquired from cone-beam computed tomography (CBCT) scans.

Although sizeable 3D scanning modality exist, developing new advanced methods and techniques involving 3D scanning for real-life forensic applications requires accessibility and practicality. The application of 3D scanning modalities, such as photogrammetry, 3D surface, and micro-XCT scanning, is frequently used in osteology and anthropology. The micro-XCT scanner is universally accepted by the scientific community as the gold standard modality [10] in providing high final resolution for external and internal structure assessment [11]. Unlike micro-XCT, photogrammetry and 3D surface scanning do not require X-rays or professional training.

Consequently, photogrammetry and 3D surface scanning have been more widely applied in several research fields such as anthropology, archaeology, medicine, and geomorphology and appear to be the ideal types of modalities to be integrated into forensic analyses [12]. Photogrammetry reconstructs the shape, colour, and texture of the surface of objects from multiple pictures [13] using a least squares algorithm [14,15]. While both modalities use the triangulation principle to estimate a point cloud and compute polygon meshes, only 3D surface scanners emit laser or structured light to capture the shape and size of an object.

Therefore, the introduction of 3D surface scanning might provide an efficient set of advanced techniques complementary to the existing metric forensic analyses. Incorporating 3D scanning modalities might allow South African forensic anthropologists to analyze the population affinity shape-related variation in a more accurate and repeatable way.

Consequently, the following question arises: how accurate is using a 3D surface scanner for forensic population affinity estimation purposes? To this end, the current study aimed to compare topographical and shape analyses of 3D surface scanned reconstructions to the same analyses of gold standard micro-XCT reconstructions.

Three-dimensional reconstructions and shape data from both scanning modalities were acquired and compared using landmark reproducibility testing, geometric discrepancies, and shape analysis using GMM.

Materials and methods

Materials

The sample consisted of 44 adult crania from the PBC, housed at the Department of Anatomy, University of Pretoria [16]. The overall age ranged between 18 and 80 years, with a mean sample age of 48 years. As this study is based on the accuracy of the population affinity estimates using shape data acquired from two different types of modalities, the South African

ancestral groups studied were black and white South Africans, each representing 22 specimens. For consistency during data collection, any condition that could affect the morphology of the crania and subsequent analysis results was excluded from the sample. Such conditions include any pathologies, trauma, surgical intervention, or deformities. Ethical clearance was obtained from the Faculty of Health Sciences Research Ethics committee of the University of Pretoria (reference number: 294/2020).

Methods

Data acquisition

Micro-CT scanner

Micro-XCT scans of the 44 crania were obtained at the South African Nuclear Energy Corporation SOC Ltd (Necsa Pelindaba, South Africa) [11]. The acquisition and reconstruction parameters of the micro-XCT scans were as follows: 90-120 kV voltage, 70-220 µ. A current, angular increment of 1000 projections per 360°, and final resolutions ranged between 0.066 and 0.100 mm. The datasets obtained in TIFF format were segmented using the Edit New Label field module of Amira-Avizo 2019.3 software (Thermo Fisher Scientific, Inc.). The threshold values between segmented components were obtained according to the "Half Maximum Height" (HMH) quantitative iterative thresholding method [17] using ImageJ software [18]. Prior to polygonization, the bone material was then partitioned and extracted from all other materials (e.g., air) or noise present in the scan using the Amira-Avizo 2019.3 software (Thermo Fisher Scientific, Inc.). It resulted in the generation of 3D reconstructions saved in polygon file format (.ply) (Fig. 1.a).

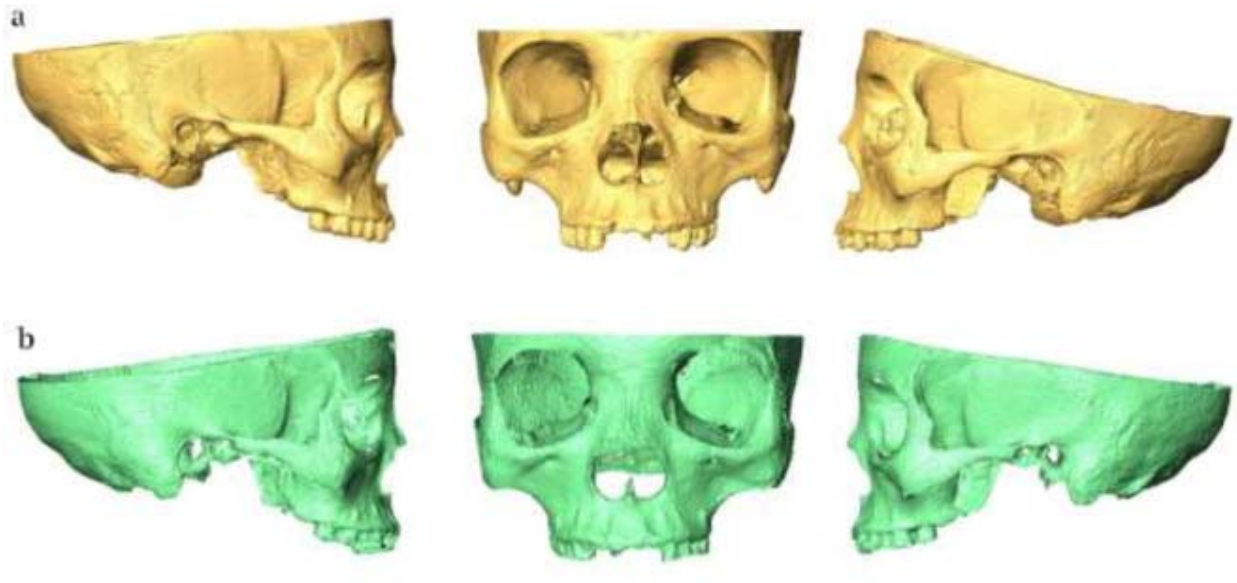

Fig. 1. 3D reconstructions of a same specimen scanned using both modalities. **a**: 3D reconstruction from Micro-CT; **b**: 3D reconstruction from 3D surface scanner.

3D surface scanner

The 44 crania were scanned using the NEXTENGINE Ultra-HD 3D scanner [19] at the University of Pretoria. Each cranium was scanned in a standard anatomical position at 360˚

using 12 divisions. All specimens were scanned at 17 inches from the front of the scanner. For each cranium, the parameters associated with the *WIDE mode* were used: accuracy =0.015"; field of view: 13.5" x 10.1"; scanning density: 29 000 points/in; dimensional accuracy: 300 microns. The texture for each cranium was also recorded (texture density: 200 DPI). However, as this study does not primarily focus on texture rendering, the texture information was not used for further analysis. Finally, no post-surface scanning processing was applied. The final 3D reconstructions were subsequently generated and extracted in polygon file format (.ply) (Fig. 1.b).

Mid-facial shape data

South African mid-facial shape variation has already been proven accurate for population affinity estimation in forensic anthropological analysis. Therefore, we applied our research to the human mid-facial region, including zygomatic, maxilla, nasal bones, and nasal aperture.

The landmarks were designed to reflect the mid-facial shape in the best possible manner. Amira-Avizo 2019.3 software (Thermo Fisher Scientific, Inc.) was utilized to place 41 landmarks (Fig. 2) on the mid-facial region manually on all 3D reconstructions obtained from both modalities. The Cartesian coordinates (x; y; z) representing mid-facial shape matrices were then recorded for statistical analysis. The definition of the landmarks used are described in Table 1.

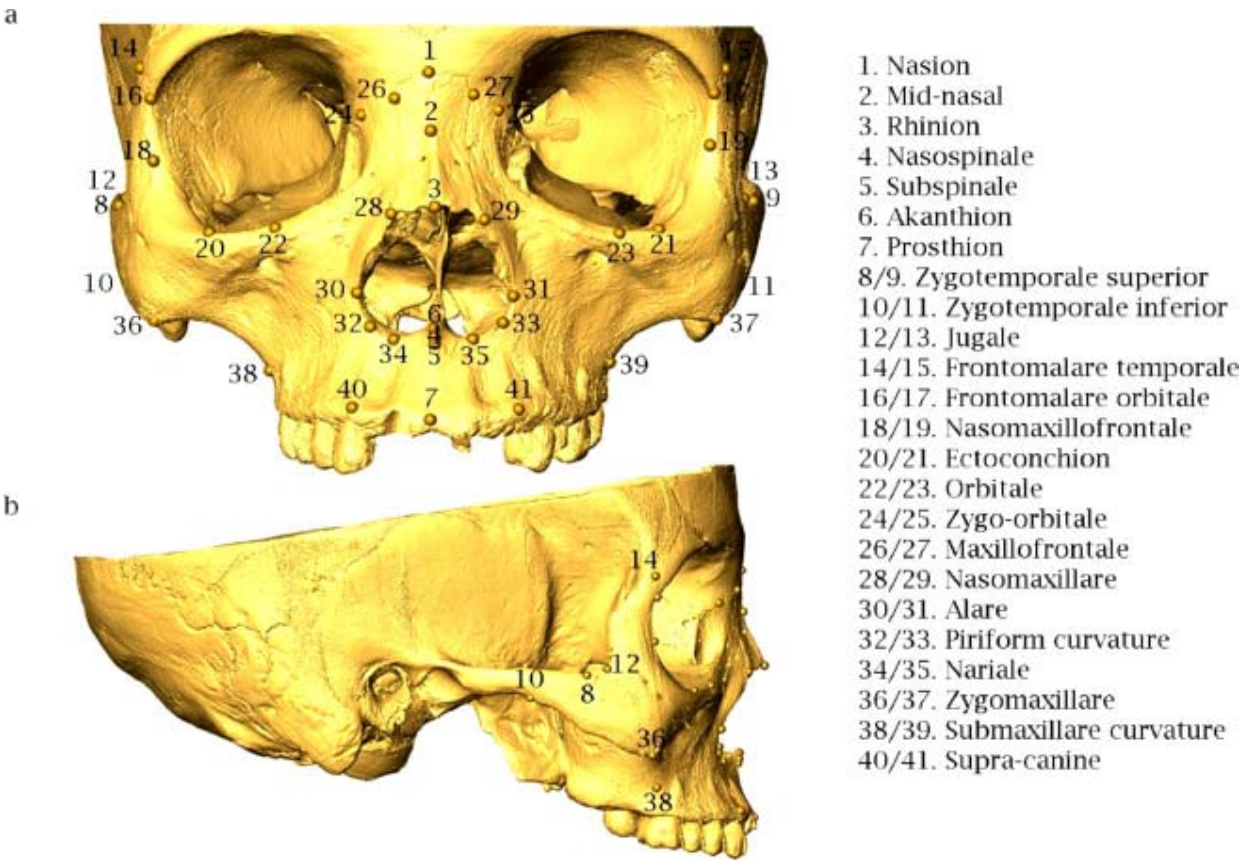

Fig. 2. Landmarks placed on the 3D reconstructions. a: frontal view; b: lateral view.

Table 1. Definition and nature of craniometric landmarks used [20]

	Landmarks	Nature	Definition
1	Nasion	Median	Intersection of the nasofrontal sutures in the median plane.
2	Mid-nasal	Median	Midline point on the internasal suture midway between nasion and rhinion.
3	Rhinion	Median	Most rostral (end) point on the internasal suture. Cannot be determined accurately if nasal bones are broken distally.
4	Nasospinale	Median	The point where a line drawn between the inferior most points of the nasal aperture crosses the median plane. Note that this point is not necessarily at the tip of the nasal spine.
5	Subspinale	Median	The deepest point seen in the profile view below the anterior nasal spine (orthodontic point A).
6	Akanthion	Median	Most anterior midline point of the nasal spine.
7	Prosthion	Median	Median point between the central incisors on the anterior most margin of the maxillary alveolar rim.
8/9	Zygotemporale superior	Bilateral	Most superior point of the zygomatico-temporal suture.
10/11	Zygotemporale inferior	Bilateral	Most inferior point of the zygomatico-temporal suture.
12/13	Jugale	Bilateral	Vertex of the posterior zygomatic angle, between the vertical edge and horizontal part of the zygomatic arch.
14/15	Frontomalar temporal	Bilateral	Most lateral part of the zygomaticofrontal suture.
16/17	Frontomalar orbitale	Bilateral	Point on the orbital rim marked by the zygomaticofrontal suture.
18/19	Nasomaxillofrontale	Bilateral	Point at the intersection of the frontal, maxillary, and nasal bones.
20/21	Ectoconchion	Bilateral	Lateral point on the orbit at a line that bisects the orbit transversely.
22/23	Orbitale	Bilateral	Most inferior point on the inferior orbital rim. Usually falls along the lateral half of the orbital margin.
24/25	Zygo-orbitale	Bilateral	Intersection of the orbital margin and the zygomaticomaxillary suture.
26/27	Maxillofrontale	Bilateral	Intersection of the anterior lacrimal crest with the frontomaxillary suture.
28/29	Nasomaxillare	Bilateral	Most inferior point of the nasomaxillary suture on the nasal aperture.
30/31	Alare	Bilateral	Instrumentally determined as the most lateral point on the nasal aperture in a transverse plan.
32/33	Piriform curvature	Bilateral	Most infero-lateral point of the piriform aperture.
34/35	Nariale	Bilateral	Most inferior point of the piriform aperture.
36/37	Zygomaxillare	Bilateral	Most inferior point onthe zygomaticomaxillary suture.
38/39	Submaxillare curvature	Bilateral	Most supero-medial point on the maxillary inflexion between the zygomaxillare and the ectomolar.
40/41	Supra-canine	Bilateral	Point on the superior alveolar ridge superior to the crown of the maxillary canine.

Statistical analysis

Comparison of landmarks reproducibility

Repeatability testing was performed to assess the reproducibility of the landmark positioning on both the gold standard micro-XCT and 3D surface scanner. The inter- and intra-observer error was assessed by placing the 41 craniometric landmarks on six randomly selected specimens scanned by the two modalities (micro-XCT and 3D surface scanner). For the inter-observer error, the landmark placements were performed twice by two different observers. For the intra-observer error, the landmark placements were performed twice by the same observer with an interval of two weeks. The reproducibility of the landmark positioning was calculated

using the dispersion Δ_{ij} for each landmark *i* and individual *j*. Dispersion is defined as the Mean Euclidean Distance (MED) of the sample landmark p_{ijk} to the mean $\bar{p}_{ij}$ of the (x, y, z)-coordinates of landmark *i* over all observations *k* (inter, intra, resp.) for subject *j (Formula 1)*:

$$\Delta_{ij} = \sum_{k=1}^{K} \left\| p_{ijk} - \bar{p}_{ij} \right\| / K, \text{ with} \bar{p}_{ij} = \sum_{k=1}^{K} p_{ijk} / K \quad (1)$$

Boxplots of MED values were generated to show the variation of dispersion over different subjects. Global precision is reported as the global (averaged over all landmarks) mean (μ_{Δ}) and median (m_{Δ}) of the per landmark mean ($\mu_{\Delta i}$) and median ($m_{\Delta i}$) values (over all subjects).

Visualisation of the geometric discrepancies

Visualization of geometric discrepancies was performed between the gold standard micro-XCT and 3D surface scanner. The 3D reconstructions from both modalities were superimposed and placed in the same coordinate system through image registration. The mentioned steps allowed for the alignment of each 3D reconstruction to the gold standard micro-XCT reconstruction. The distance between the two data sets from the micro-XCT and the 3D surface reconstructions were minimized through an iterated closest points algorithm [21]. In this study, 100 iterations were used to minimize the distance between points of two raw data sets for the micro-XCT and 3D surface reconstructions. Thereafter, the surface distance between the 3D surface reconstructions was calculated with a maximum distance of 5 mm. Then, the geometric discrepancies were displayed using the color map module on Amira-Avizo 2019.3 software (Thermo Fisher Scientific, Inc.). This software creates color maps that aid in the location of maximum differences, which was utilized to display the topography of the geometric discrepancies, thereby allowing the maximum differences to be located. The color map (in mm) ranges from blue to red, with the smallest discrepancies represented by blue (0 mm), and red representing the most significant discrepancies (5 mm). The minimum to maximum distances expressed in absolute values were represented by the lower and upper extremities observed between the micro-XCT and 3D surface reconstructions.

Comparison of population affinity shape analysis

A population affinity shape analysis was visualized on matrices acquired from both modalities, and the results were then compared. A Generalized Procrustes Analysis (GPA) was performed on the Cartesian coordinates to obtain orientation-invariant shape coordinates [22,23]. A principal component analysis (PCA) was performed to assess population affinity-related shape variations between both modalities by creating independent transformed variables referred to as principal component (PC) scores. Before applying statistical testing, the PC scores distribution was analyzed using a multivariate normality test conducted through the interpretation of Q-Q plots to allow for the presumption that the variables are distributed according to the distribution tested [24]. All results were double-checked using parametric and non-parametric testing, and only if both tests provided a similar outcome were the results considered reliable. Parametric (one-way ANOVA) and non-parametric tests (permutation testing) were employed to assess the influence of population affinity on mid-facial shape variation. Thereafter, for classification purposes, the standard Discriminant Function Analysis (DFA) was performed. An analysis of Variance (ANOVA) was conducted using the Procrustes ANOVA function in the geomorph package in R [25].

This function allows for the quantification of shape variation attributable to population affinity in a linear model and estimates the probability of this variation ("significance") for a null model via distributions generated from resampling permutations. For the sake of accuracy, the results were double-checked using permutation tests (non-parametric tests). The chosen factor (population affinity) was calculated and compared to values obtained from the sample, randomly and repeatedly assigned. The number of resampled values that surpassed the "true" value is divided by the total number of permutation rounds (10,000 rounds). The null hypothesis cannot be rejected if the value falls within the range of random grouping and if the measurement values do not exceed the one generated by chance [26], [27], [28]. It must be acknowledged that permutation testing has less statistical power than parametric testing. Finally, to assess the discriminative power of population affinity, a Discriminant function analysis (DFA) was also conducted, and the results were validated using leave-one-out cross-validation [27,28]. The permutation tests and the DFA were conducted using morpho R-package functions [28]. All statistical analyses performed in this study were done on R-studio v 1.0.44-®2009-2016 for Windows [29].

Results

Inter- and intra-observer errors (Fig. 3) were calculated from 41 landmarks placed on six random specimens scanned with both modalities. The means (μ Δ) for both micro-XCT and 3D surface scans were 1.137 and 0.829 mm for intra-observer error and 0.568 and 1.254 mm for inter-observer error, respectively. For both inter-and intra-observations on the Micro-CT reconstructions, the left and right *Orbitale* (landmarks 22 and 23) had the highest dispersion values. On the other hand, *Rhinion* and *left Nasomaxillare* (landmarks 3 and 28) demonstrated the lowest dispersion values. On the 3D surface scans, the left and right *Submaxillare curvature* (landmarks 38 and 39) had the highest dispersion values, with the *Zygotemporale superior (landmarks 8 and 9)* showing the lowest dispersion values for both intra and inter-observer.

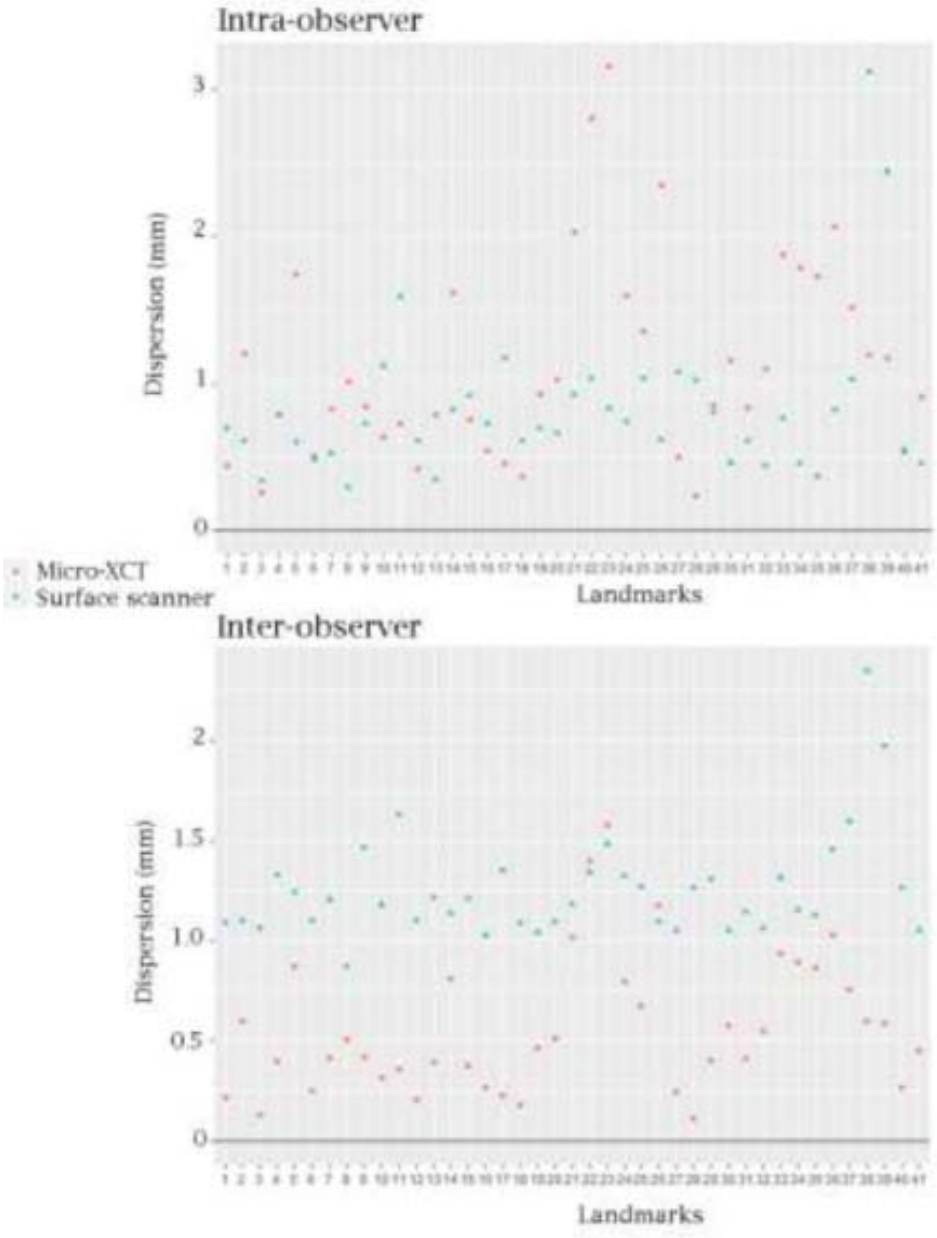

Fig. 3. Graphical representations of the dispersion in mm per landmark over all subjects.

The topographical analysis on the same six random specimens showed minor differences of the mid-facial region analyzed across both modalities (Fig. 4). Interestingly, the slight differences (visible as green) found on the maxilla, the postero-lateral margin of the zygomatic and the frontal process areas were consistent with the findings obtained from the landmarks that differed between micro-XCT and 3D surface reconstructions.

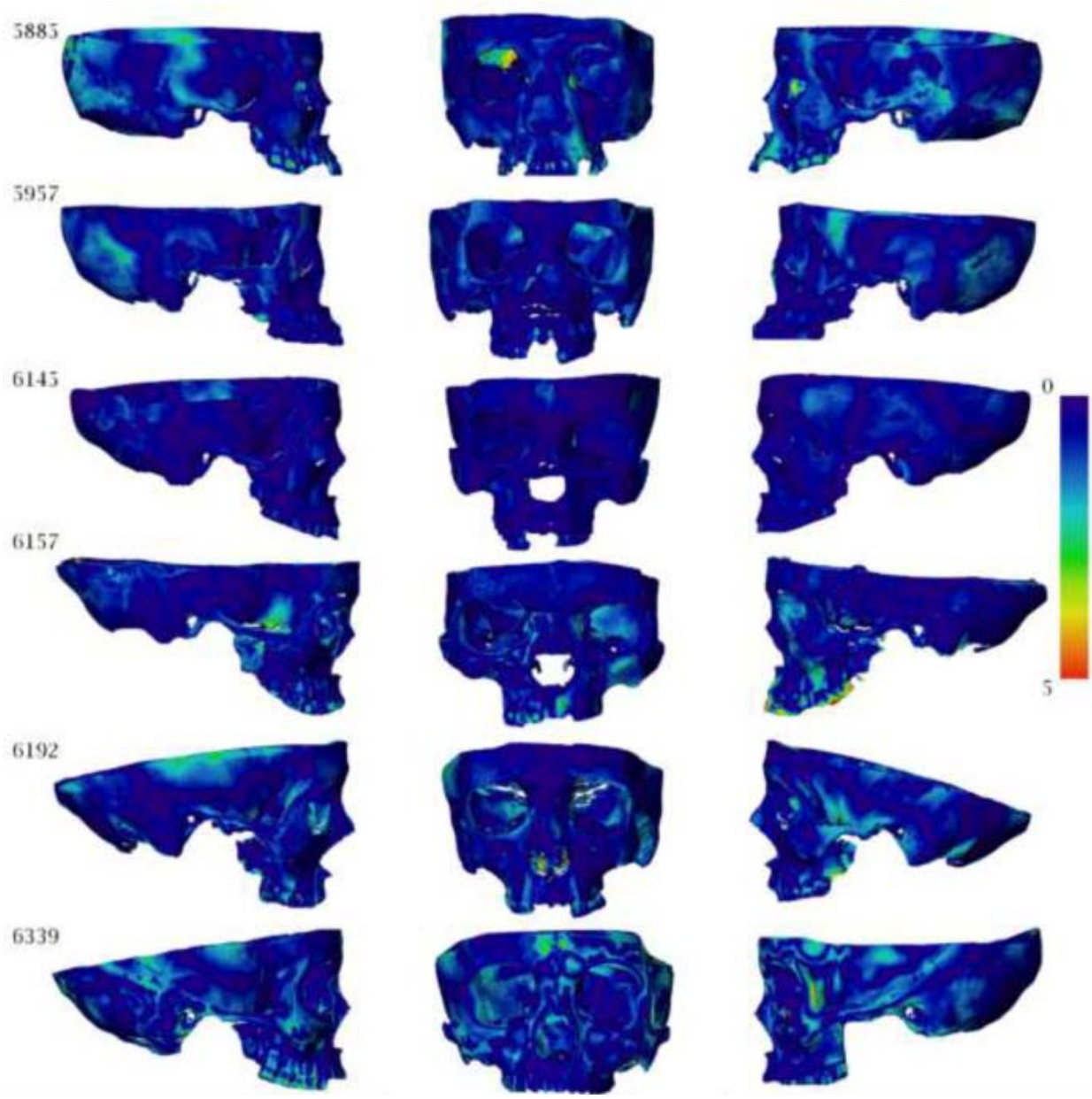

Fig. 4. Surface-based comparison of six random 3D surface reconstruction**s** in alignment with that the micro-XCT. The color map (in mm) starts with blue (minimum distances (0 mm)), then passes through yellow, and ends with red (maximum distances (5 mm)).

When the landmark shape coordinates were analyzed with PCA (Fig. 5), the results showed similar population affinity-related mid-facial shape variations between both modalities, with an analogous clustering (Fig. 5) between the two ancestral groups studied. For both reconstruction modalities, the multivariate normality analyses, using Q-Q plots of Mahalanobis distances, revealed a slight deviation from the expected normal distribution. For the sake of accuracy, all results were double examined using both parametric and non-parametric tests, and the results were only considered reliable if both tests provided a similar outcome. For both Micro-CT and 3D surface reconstructions, the statistical analysis was performed on the first 24 PC-scores of the shape component. The variance was associated with the linear model "shape against population affinity," explained 95.5% of overall shape variation (Micro-CT: Anova:

P=4.57e-11, Permutation testing: P=0.001; 3D Surface scanner: Anova: P=1.17e-11, Permutation testing: P=0.001). For the Micro-CT reconstructions, cross-validated DFA produced a correct classification rate of 100% for black South Africans and 94.11% for white South Africans (with the overall accuracy being 97.5%). We double-checked this result by calculating a between-group PCA, using population affinity as a grouping variable. The resulting accuracy was slightly lower, with a correct classification of 91.30% for black South Africans and 88.23% for white South Africans (with the overall accuracy being 97.5%). For the 3D surface scanner, cross-validated DFA produced a correct classification rate of 100% for black South Africans and was slightly lower compared to Micro-CT findings with 88.25% for white South Africans (with the overall accuracy being 95%). The results were also double-checked by calculating a between-group PCA, using population affinity as a grouping variable. The resulting accuracy was slightly lower, with a correct classification of 95.65% for black South Africans and 88.23% for white South Africans (with the overall accuracy being 92.5%).

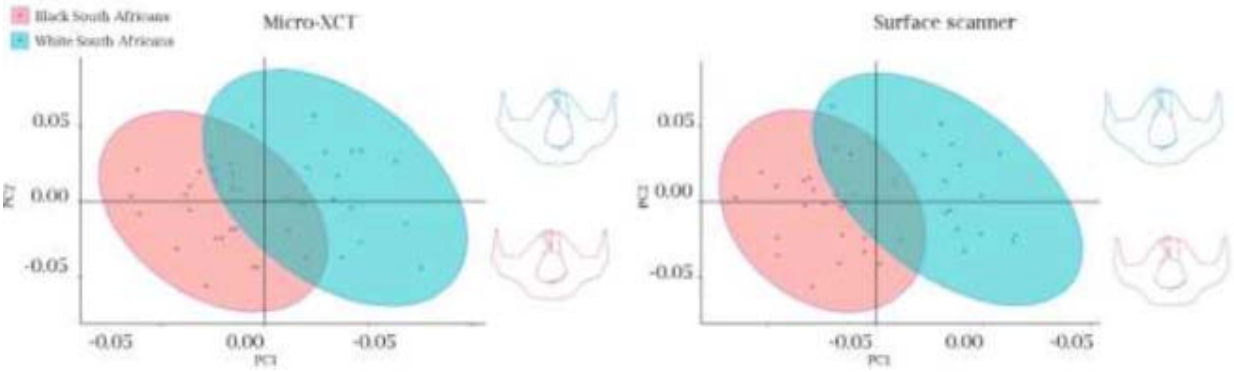

Fig. 5. Principal component analysis (PCA) and consensus mid-face shape variations related to population affinity based on landmark shape coordinates collected on 3D reconstructions from both modalities.

Discussion

The purpose of the present research was to assess the reliability of 3D surface scanning topographical and shape analysis in comparison to Gold standard micro-XCT reconstructions.

Both scanning modalities provided relatively similar landmark datasets, which was consistent with previous studies [12,30,31]. The landmark reproducibility testing showed minimal dispersion errors for both datasets, indicating that the placement of landmarks on 3D reconstructions from both modalities was reliable and repeatable. However, a degree of observer experience is required when placing landmarks on 3D reconstructions acquired by surface scanning, as some sutures were not easily identifiable, such as the *Zygotemporale superior* and *inferior, Zygo-orbitale*, and *Zygomaxillare*. The results of the topographical analysis showed that micro-XCT and 3D surface scanning yielded similar 3D mesh reconstructions with only slight differences found between surface models on the maxilla, the postero-lateral margin of the zygomatic and frontal process areas. The minimal geometric discrepancies observed between the reconstructions also suggested that both modalities will provide similar shape landmark datasets, and both can be used without compromising the accuracy of analyses. The statistical findings showed similar population affinity-related mid-facial shape variations analyzed across both modalities using GMM. The PCA revealed a similar clustering of both landmarks' configurations between the two modalities, emphasizing

that the two-scanning procedure provided relatively similar shape data and similar shape analysis for population affinity-related shape variations.

Accessibility and practicality are required when developing innovative 3D scanning approaches for real-life applications in forensic analysis.

To this end, the utilization of a micro-XCT scanning modality could be counterproductive and a challenging process to integrate in forensic analyses due to the cost and the time generated. Moreover, the use of micro-XCT scanners comes with strict safety regulations because of the utilization of X-ray tomography [11] involving limited accessibility to individuals not trained, such as forensic anthropologists. Photogrammetry and 3D surface scanning modalities, in comparison with micro-XCT, do not require X-rays or professional instruction. Consequently, they appear to be the ideal modality to be integrated into forensic analyses by making the scanning procedure more accessible and easier to utilize for forensic anthropologists.

Further, in contrast to 3D surface scanners, most photogrammetric procedures capture only shape information, raising a main limitation in its practicability and accuracy in its utilization into a forensic analysis procedure. Indeed, unless metadata of the internal geometry of the camera used is included in the procedure or if the 3D reconstruction from the photogrammetry is manually calibrated based on a scale placed next to the object during scanning [32], the procedure will capture only the shape component. Finally, the 3D surface scanner has proven to be more consistent in 3D reconstruction generation than photogrammetry software packages [12]. The generation of 3D reconstruction differs enormously in quality depending on the types of photogrammetry software used [12]. Consequently, the emergence of 3D surface scanning technology may provide an efficient source for developing innovative techniques that enhance the current forensic analysis.

Current morpho-phenotyping analysis tools (eg., FORDISC 3) restrict the analyses to traditional craniometric analyses using inter-landmark distances; GMM analyse the statistical properties of ensembles of 3D landmark coordinates. Here, the variation and co-variation of the landmark coordinates with respect to a standard archetype shape, such as the population mean, is studied. Generalized Procrustes Alignment removes the shape-irrelevant pose differences resulting in residual Procrustes coordinates studied in a linearized approximation (the tangent space) such that conventional multivariate statistical methods can be applied testing hypotheses about shapes, shape differences, and correlations. Finally, the use of GMM for population affinity estimation using the midface retains the objects' geometry and analyses subtle structural differences. Innovative 3D approaches allow forensic analysts to overcome the non-utilization of fragmented bones to create sub-specific discriminate shape configurations to analyse specific patterns not readily observable with traditional techniques. Despite the fact that new 3D imaging methods might allow forensic analysts to assess specific patterns not readily revealed by the non-metric and metric methods, they do not undermine the significance of already standardized and widely used methods in forensic anthropology. In forensic cases, real-life application, reliable, accessible, and more efficient methods using 3D imaging approaches involving practical 3D scanning modalities, accurate 3D anatomical information extraction, and advanced statistical analysis might allow South African forensic anthropologists to analyze shape-related cranial variation in a more accurate and repeatable way.

Conclusion

This study assessed the accuracy of topographical and shape analysis using 3D surface scanning compared to Gold standard micro-XCT reconstructions.

Our findings suggest that both scanning modalities yielded similar 3D mesh reconstructions and similar landmark datasets to analyze population affinity-related mid-facial shape variations. Our results indicated that 3D surface scanning modalities could be utilized for forensic population affinity estimation purposes. However, more extensive research is required, with a larger sample size, including more population groups, to substantiate this study's findings. In addition, incorporating 3D scanning modalities and advanced GMM into existing osteometry methods will allow South African forensic anthropologists to analyze morphological variations more accurately and repeatably. Finally, it will enable forensic anthropologists to provide a more efficient biological profile to solve forensic cases and improve existing analyses.

Funding

This work was supported by the Bakeng se Afrika grant, Erasmus+ KA2 Capacity Building in Higher Education Project N. _597924-EPP-1-2018-1-ZA-EPPKA2-CBHE-JP.

Ethics approval

Ethical clearance was obtained from the Ethics Committee, Faculty of Health Sciences, University of Pretoria (reference number: 294/2020).

CRediT authorship contribution statement

AF Ridel: Conceptualization, Data curation, Formal analysis, Funding acquisition, Investigation, Methodology, Project administration, Software, Validation, Visualization, Writing – original draft, Writing – review & editing. **N.P. Bothma:** Data curation, Writing – review & editing. **L. Liebenberg:** Conceptualization, Validation, Writing – review & editing. **AC Oettlé:** Resources, Software, Validation, Writing – review & editing. **EN L'Abbe:** Conceptualization, Funding acquisition, Project administration, Resources, Supervision, Validation, Writing – review & editing.

Declaration of Competing Interest

The authors declare that they have no known competing financial interests or personal relationships that could have appeared to influence the work reported in this paper.

Acknowledgments

The authors would like to acknowledge the curator of the Pretoria Bone Collection at the Department of Anatomy of the University of Pretoria, Ms. Gabriele C. Krüger, for the access to the bone and the micro-XCT specimens. Ethical clearance was obtained from the Faculty of Health Sciences Research Ethics committee of the University of Pretoria (reference number: 294/2020). We are thankful to the Sefako Makgatho Health Sciences University, Ga-Rankuwa, Pretoria, South Africa, to access the surface scanner. We acknowledge Bakeng se

Afrika, coordinated by Prof. Ericka N. L'Abbé (University of Pretoria, Pretoria, South Africa) and Prof. Anna Oettlé (Sefako Makgatho Health Sciences University, Ga-Rankuwa, Pretoria, South Africa) for the financial support.

References

[1] Y. Sobuwa, There are over 900 unclaimed bodies in Gauteng mortuaries, City Press, March 31, 2023 (n.d.), https://www.news24.com/citypress/news/there-are-over-900-unclaimed-bodies-in-gauteng-mortuaries-20230227. accessed.

[2] K.E. Stull, M.W. Kenyhercz, E.N. L'Abbé, Ancestry estimation in South Africa using craniometrics and geometric morphometrics, Forensic Sci. Int. 245 (2014) 206. e1–206.e7, a.

[3] K. Krishan, P.M. Chatterjee, T. Kanchan, S. Kaur, N. Baryah, R.K. Singh, A review of sex estimation techniques during examination of skeletal remains in forensic anthropology casework, Forens. Sci. Int. 261 (2016) 165.e1–165.e8, https://doi.org/10.1016/j.forsciint.2016.02.007.

[4] F.L. Bookstein, Morphometric Tools for Landmark Data: Geometry and Biology, Cambridge Univ. Press, Cambridge, 1997. Reprint.

[5] J.L. McDowell, E.N. L'Abbé, M.W. Kenyhercz, Nasal aperture shape evaluation between black and white South Africans, Forens. Sci. Int. 222 (1) (2012) 397–3e1, https://doi.org/10.1016/j.forsciint.2012.06.007.

[6] J.L. McDowell, M.W. Kenyhercz, E.N. L'Abbé, An evaluation of nasal bone and aperture shape among three South African populations, Forens. Sci. Int. 252 (2015) 189–1e1, https://doi.org/10.1016/j.forsciint.2015.04.016.

[7] A.F. Ridel, F. Demeter, J. Liebenberg, E.N. L'Abbé, D. Vandermeulen, A.C. Oettlé, Skeletal dimensions as predictors for the shape of the nose in a South African sample: a cone-beam computed tomography (CBCT) study, Forens. Sci. Int. 289 (2018) 18–26, https://doi.org/10.1016/j.forsciint.2018.05.011.

[8] A. Ridel, F. Demeter, M. Galland, E. L'Abbé, D. Vandermeulen, A. Oettlé, Automatic landmarking as a convenient prerequisite for geometric morphometrics. Validation on cone beam computed tomography (CBCT)- based shape analysis of the nasal complex, Forens. Sci. Int. 306 (2020), 110095, https://doi.org/10.1016/j.forsciint.2019.110095.

[9] A.F. Ridel, F. Demeter, E.N. L'Abbé, D. vandermeulen, A.C. Oettlé, Nose approximation among South African groups from cone-beam computed tomography (CBCT) using a new computer-assisted method based on automatic landmarking, Forens. Sci. Int. 313 (2020), 110357, https://doi.org/10.1016/j.forsciint.2020.110357 b.

[10] A.J. Burghardt, T.M. Link, S. Majumdar, High-resolution computed tomography for clinical imaging of bone microarchitecture, Clin. Orthopaed. Rel. Res. 469 (2011) 2179–2193, https://doi.org/10.1007/s11999-010-1766-x.

[11] J.W. Hoffman, F.C. De Beer, Characteristics of the Micro-Focus X-ray Tomography Facility (MIXRAD) at Necsa in South Africa, in: 18th World Conference on Nondestructive Testing. South African Nuclear Energy Corporation (Necsa), Durban, South Africa, 2012.

[12] L. Waltenberger, K. Rebay-Salisbury, P. Mitteroecker, Three-dimensional surface scanning methods in osteology: a topographical and geometric morphometric comparison, Am J Phys Anthropol 174 (2021) 846–858, https://doi.org/10.1002/ajpa.24204.

[13] K. Kraus, I. Harley, Photogrammetry: Geometry from Images and Laser Scans, 2. ed, de Gruyter, Berlin, 2007.

[14] A. Evin, T. Souter, A. Hulme-Beaman, C. Ameen, R. Allen, P. Viacava, G. Larson, T. Cucchi, K. Dobney, The use of close-range photogrammetry in zooarchaeology: Creating accurate 3D models of wolf crania to study dog domestication, J. Archaeol. Sci.: Rep. 9 (2016) 87–93, https://doi.org/10.1016/j.jasrep.2016.06.028.

[15] H. Rüther, J. Smit, D. Kamamba, A comparison of close-range photogrammetry to terrestrial laser scanning for heritage documentation, South Afric. J. Geomatic. 1 (2012) 149–162, https://doi.org/10.4314/sajg.v1i2.

[16] E.N. L'Abbé, M. Loots, J.H. Meiring, The Pretoria Bone Collection: a modern South African skeletal sample, HOMO 56 (2005) 197–205, https://doi.org/10.1016/j.jchb.2004.10.004.

[17] C.F. Spoor, F.W. Zonneveld, G.A. Macho, Linear measurements of cortical bone and dental enamel by computed tomography: Applications and problems, Am. J. Phys. Anthropol. 91 (1993) 469–484, https://doi.org/10.1002/ajpa.1330910405.

[18] C.A. Schneider, W.S. Rasband, K.W. Eliceiri, NIH Image to ImageJ: 25 years of image analysis, Nat. Methods 9 (2012) 671–675, https://doi.org/10.1038/nmeth.2089.

[19] NextEngine 3D Scanner ULTRA HD review - 3D scanner [WWW Document], 2020. Aniwaa. https://www.aniwaa.com/product/3d-scanners/nextengine-3d-scanner-ultra-hd/(accessed 4.15.20).

[20] J. Caple, C.N. Stephan, A standardized nomenclature for craniofacial and facial anthropometry, Int. J. Legal Med. 130 (2016) 863–879, https://doi.org/10.1007/s00414-015-1292-1.

[21] P.J. Besl, N.D. McKay, A method for registration of 3-D shapes, IEEE Trans. Pattern Anal. Mach. Intell 14 (1992) 239–256.

[22] D.E. Slice, Geometric Morphometrics, Annu. Rev. Anthropol. 36 (2007) 261–281, https://doi.org/10.1146/annurev.anthro.34.081804.120613.

[23] L. Dryden, K.V. Mardia, Statistical Shape Analysis, John Wiley and Sons, Chichester, 1998.

[24] L. Scrucca, Assessing Multivariate Normality through Interactive Dynamic Graphics 2000.

[25] Adams, D., Collyer, M., & Kaliontzopoulou, A. Geometric morphometric analyses of 2D/3D landmark data (2018).

[26] S. Schlager, Soft-tissue reconstruction of the human nose: population differences and sexual dimorphism = Weichteilrekonstruktion der menschlichen Nase: Populationsunterschiede und Sexualdimorphismus, Universit¨at, Freiburg, 2013.

[27] S. Schlager, A. Rüdell, Analysis of the human osseous nasal shape—population differences and sexual dimorphism, Am. J. Phys. Anthropol. 157 (2015) 571–581, https://doi.org/10.1002/ajpa.22749. Doi:2015.

[28] S. Schlager, Calculations and visualisations related to geometric morphometrics (2020).

[29] R Core Team., R: A Language and Environment for Statistical Computing, R Foundation for Statistical Computing, Vienna, Austria, 2002. http://www.R-project.org.

[30] M. Friess, Calvarial shape variation among Middle Pleistocene hominins: an application of surface scanning in palaeoanthropology, Comptes Rendus Palevol 9 (2010) 435–443, https://doi.org/10.1016/j.crpv.2010.07.016.

[31] M. Friess, Scratching the Surface? The use of surface scanning in physical and paleoanthropology, J. Anthropol. Sci. (2012) 1–26, https://doi.org/10.4436/jass.90004.

[32] M.Á. Maté González, J. Yravedra, D. González-Aguilera, J.F. Palomeque-González, M. Domínguez-Rodrigo, Micro-photogrammetric characterization of cut marks on bones, J. Archaeologic. Sci. 62 (2015) 128–142, https://doi.org/10.1016/j.jas.2015.08.006.